

---

# A Topology Layer for Machine Learning

---

Rickard Brüel-Gabrielsson<sup>1,2</sup> Bradley J. Nelson<sup>1,3</sup> Anjan Dwaraknath<sup>1</sup> Primoz Skraba<sup>4</sup>  
Leonidas J. Guibas<sup>1</sup> Gunnar Carlsson<sup>1,2</sup>

<sup>1</sup>Stanford University <sup>2</sup>Unbox AI <sup>3</sup>Stanford Linear Accelerator <sup>4</sup>Queen Mary University of London  
rbg@cs.stanford.edu, {bradnelson, anjandn}@stanford.edu,  
p.skraba@qmul.ac.uk, {guibas, carlsson}@stanford.edu

## Abstract

Topology applied to real world data using persistent homology has started to find applications within machine learning, including deep learning. We present a differentiable topology layer that computes persistent homology based on level set filtrations and distance-bases filtrations. We present three novel applications: the topological layer can (i) serve as a regularizer directly on data or the weights of machine learning models, (ii) construct a loss on the output of a deep generative network to incorporate topological priors, and (iii) perform topological adversarial attacks on deep networks trained with persistence features. The code<sup>1</sup> is publicly available and we hope its availability will facilitate the use of persistent homology in deep learning and other gradient based applications.

## 1 Introduction

Persistent homology, or simply persistence, is a well-established tool in applied and computational topology. In a deep learning setting, persistence has mainly been used as preprocessing to provide topological features for learning [27, 16, 21]. There has been work that uses differentiable properties of persistence to incorporate topological information in deep learning [22, 10] and regularization [8]; however, such work has focused on specialized applications and specific functions of the persistence diagrams. Another line of work uses applied topology and persistence for deep learning interpretability [3, 13], automating the construction of deep learning architectures [5], complexity measures [19, 24], and adversarial attacks [14, 15]. Persistence fits naturally in geometric problems and has been applied to a number of geometry processing applications including shape matching [6], optimal pose-matching [11], shape segmentation [28], and surface reconstruction [4]. In [4] gradient descent was successfully applied to persistence-based optimization. In this work, we translate this idea to the domain of machine learning and deep learning. This provides an easy-to-use and general way to incorporate topological priors in many machine learning settings.

In many deep learning settings there is a natural topological perspective. This is true both for images and for 3D data such as point clouds or voxel spaces. In fact, many of the failure cases of generative models are topological in nature [32, 18]. We show how topological priors can be used to improve such models. It has been speculated [3, 5] that models that rely on topological features might have desirable properties besides test accuracy; one such property has been robustness against adversarial attacks [7]. However, to our knowledge, no such attacks have been conducted. With our layer, such attacks are easy to implement, and we provide illustrative examples. As a language for describing global properties of data, topology is also useful in exploring properties of generalization. There are some natural measures of topological simplicity (akin to norm regularization) and we show how these can successfully be used to regularize the parameters or weights of machine learning models.

---

<sup>1</sup><https://github.com/bruel-gabrielsson/TopologyLayer>

A summary of our contributions is: (i) an easy-to-use persistence layer for level sets, Rips filtrations, and (weak) Alpha filtrations, (ii) the first regularization using persistence on the weights of machine learning models, (iii) the first incorporation of topological priors in deep generative networks in image and 3D data settings, and (iv) the first topological adversarial attacks.

## 2 Topological Preliminaries

This section contains a review of the relevant topological notions, including persistent homology, providing an intuitive idea with some of the more technical details provided in the supplementary material. For readers who are unfamiliar with persistence, we refer the reader to a number of excellent introductions and surveys which are available [12] and [23, 4] for related work on optimizing over persistence diagrams.

**Homology groups** are a way of studying the properties of a space through *algebraic invariants*. Each dimension  $k$  has a homology group and its rank determines the number of  $k$ -dimensional features of the space. For example, the 0-dim homology counts the number of connected components, 1-dim the number of holes, 2-dim the number of voids, and so on. We restrict ourselves to *simplicial homology* although the techniques we describe are more generally applicable. We always consider geometric simplicial complexes, where the vertices correspond to points in some ambient space, e.g.  $\mathbb{R}^d$ , although the simplices need not be embedded in the space.

**Persistent homology** studies an increasing sequence of simplicial complexes or filtration,  $\emptyset = \mathcal{X}_0 \subseteq \mathcal{X}_1 \subseteq \dots \subseteq \mathcal{X}_n = \mathcal{X}$ . We consider sublevel set filtrations of a function  $f : \mathcal{X} \rightarrow \mathbb{R}$ . The filtration is defined by increasing the parameter  $\alpha$ , with  $\mathcal{X}_\alpha = f^{-1}(-\infty, \alpha]$ . Conversely, we can consider the superlevel set filtration by decreasing  $\alpha$  and defining  $\mathcal{X}_\alpha = f^{-1}[\alpha, \infty)$ . The only requirement is that each  $\mathcal{X}_\alpha$  is a simplicial complex.

The homology of the filtration is described by a *persistence diagram*. A  $k$ -dimensional persistence diagram,  $\text{PD}_k$ , is a multi-set of points in  $\mathbb{R}^2$ . Each point,  $(b, d)$  represents a  $k$ -dimensional topological feature which appears when  $\alpha = b$  and disappears<sup>2</sup> when  $\alpha = d$ . These are called the the birth time and death time respectively. Alternatively, we can view the persistence diagram as a map from a filtration to a set of points in  $\mathbb{R}^2$ :

$$\text{PD}_k : (\mathcal{X}, f) \rightarrow \{b_i, d_i\}_{i \in \mathcal{I}_k}$$

As a notational convenience, we assume that the indexing of the points is by decreasing *lifetimes*, i.e.  $d_i - b_i \geq d_j - b_j$  for  $i < j$ . An intuitive way to understand this machinery is to consider a filtration where simplices are added one at a time. It is a standard but non-obvious result that a  $k$ -dimensional simplex either creates a  $k$ -dimensional feature or destroys a  $(k - 1)$ -dimensional feature. The persistence diagram captures the pairing of these events which are represented by a pair of simplices  $(\sigma, \tau)$ , where  $b = f(\sigma)$  and  $d = f(\tau)$ . This allows us to define an inverse map

$$\pi_f(k) : \{b_i, d_i\}_{i \in \mathcal{I}_k} \rightarrow (\sigma, \tau) \quad (1)$$

Note that this map is generally not unique and must be defined carefully – see the supplementary material for details. As persistence diagrams are a collection of points in  $\mathbb{R}^2$ , there are many notions of distances between diagrams and cost functions on diagrams which depend on the points. We use loss functions that can be expressed in terms of three parameters

$$\mathcal{E}(p, q, i_0; \text{PD}) = \sum_{i=i_0}^{\infty} |d_i - b_i|^p \left(\frac{d_i + b_i}{2}\right)^q \quad (2)$$

The parameters  $p$  and  $q$  define a polynomial function, following those introduced in [2]. We sum over lifetimes beginning with the  $i_0$  most persistent point in the diagram. For example, if  $i_0 = 2$ , we consider all but the most persistent class. We also use the Wasserstein distance between diagrams – this is defined as the optimal transport distance between the points of the two diagrams. One technicality is that the two diagrams may have different cardinalities, which is why points may be mapped to the diagonal – see the supplementaty material for details.

**Optimization:** Given an input, we can compute the gradient of a loss function of a diagram. The existence of the inverse map in Equation 1 allows for the computation of a gradient, enabling

<sup>2</sup>The feature becomes trivial, e.g. a hole gets filled in.

backpropagation and the development of topological layers for neural networks. In each case, we assume the filtration is parameterized or for any choice of parameters we obtain a filtration.

We use two different types of filtrations: (1) a sub/superlevel set filtration where a function is defined on a fixed simplicial complex  $\mathcal{X}$ , and (2) a distance-based filtration whose input are points embedded in some ambient space. We refer to (1) as levelset persistence. As an example, we consider images where superlevel set filtrations are more natural. The underlying complex is the collection of pixels and the function is given by the pixel values, i.e. the superlevel set are all pixels whose value is greater than some  $\alpha$ . If we represent each pixel by a vertex and triangulate  $\mathbb{R}^2$ , the value of a simplex is given by the minimum of pixel values of vertices in the simplex. This defines a map  $\omega_{ls}(\sigma) = \operatorname{argmin}_{v \in \sigma} f(v)$  from each simplex to a vertex/pixel. Composing with  $\pi_f$ , we obtain a map from a point in the diagram to a pair of pixels – evaluating the gradients at these pixels gives the gradient with respect to the diagram via the chain rule.

In our other scenario, the input consists of points in  $\mathbf{R}^d$ . One construction for this situation is the Rips filtration,  $\mathcal{R}_\alpha$ . A Vietoris-Rips complex is constructed in two steps. First, connect all pairs of points  $(x, y)$  if  $\|x - y\| < \alpha$ . Then take the resulting graph and construct the *clique complex* by filling in all possible simplices, which correspond to cliques in the graph. In this setting, the filtration function is defined as  $f(\sigma) = \max_{(v,w) \in \sigma} \|v - w\|$  and the corresponding inverse map is  $\omega_{\mathcal{R}}(\sigma) = \operatorname{argmax}_{(v,w) \in \sigma} \|v - w\|$ . This relies on the points being embedded – extending this definition to a general metric space would require additional work. Again composing with  $\pi_f$  gives potentially four points and the gradient can be evaluated at those four points. The Rips filtration can often become too large to compute efficiently. Rather than connect all pairs of points which are sufficiently close, we take as the graph a subset of the Delaunay graph. We refer to this as the *weak Alpha filtration*. With the maps defined the derivation of the gradient is straightforward application of the chain rule.

### 3 Applications

#### 3.1 Topological Noise Reduction and Regularization

We first demonstrate how functions of persistence diagrams can be effectively used for both optimization of the placement of points, and optimization of functions on a space. We show how one can encourage the formation of lines, clusters, or holes in a set of points using geometric filtrations. We then show how level set filtrations can effectively be used for regularization of parameters in a model by penalizing the number number of local maxima in the parameter topology.

In Section 1, we reviewed several examples which use specific topological loss functions for certain applications. There are many possible losses which may be considered, and here we demonstrate some of the variety of behaviors that can be promoted using persistence. In Figure 1, we see how a set of 100 random points in the unit square can be moved into different configurations by taking gradients of different functions of the birth-death pairs in a weak-Alpha persistence diagram. In Figure 2 we see how points that are sampled from a 3D chair can be moved around using similar functions of the birth-death pairs of a Rips persistence diagram. An analysis of the optimality of one choice over another in any given situation is beyond the scope of this work. We primarily wish to draw attention to the wide variety of behaviors that can be encouraged by varying the choice of function.

Direct optimization on the filtration is not limited to geometric complexes. In Figure 3, we also optimize functions on a space. As we will see further in Section 3.2, limiting the number of local maxima in an image can improve the visual quality of generated digits. In this example, we perform optimization directly on the level sets of a noisy image to produce one that has a single global maximum, removing several noisy pixels and filling in gaps in the digit.

While these examples are illustrative, we wish to see how we can use topology directly in a

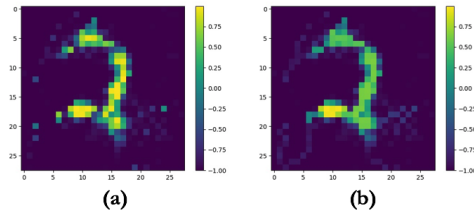


Figure 3: (a) A noisy image of the digit ‘2’. (b) after promoting a single local maximum using  $\mathcal{E}(1, 0, 2; \text{PD}_0)$

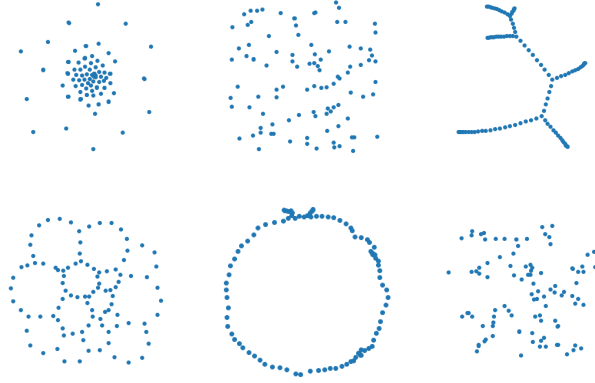


Figure 1: weak Alpha filtrations. Top center: points sampled uniformly from the unit square, Top left: Optimizing to increase  $\mathcal{E}(2, 0, 2; PD_0)$ , Top right: Optimizing to decrease  $\mathcal{E}(2, 0, 2; PD_0)$ . Bottom Left: Optimizing to increase  $\mathcal{E}(2, 0, 1; PD_1)$ , Bottom Right: optimizing to decrease  $\mathcal{E}(2, 0, 1; PD_1)$ , Bottom center: optimizing to increase  $\mathcal{E}(2, 1, 1; PD_1)$ , decrease  $\mathcal{E}(2, 0, 2; PD_0)$

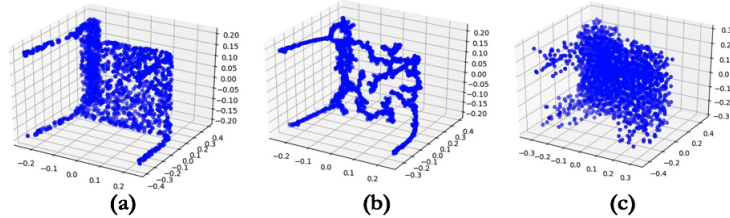


Figure 2: Rips filtrations. (a) points sampled from a chair (b) optimized to decrease  $\mathcal{E}(1, 0, 2; PD_0)$ , (c) increase  $\mathcal{E}(1, 0, 2; PD_0)$ .

machine learning model for the purposes of regularization, or encoding a prior on some topological structure.

Regularization is used throughout machine learning to prevent over-fitting, or to solve ill-posed problems. In a typical problem, we observe data  $\{X_i\}$  and responses  $\{y_i\}$ , and we would like to fit a predictive model with parameters  $\hat{\beta}$  that will allow us to make a prediction  $\hat{y}_i = f(\hat{\beta}; X_i)$  for each observation. The quality of the model is assessed by a loss function  $\ell$ , such as the mean squared error. However, many models are prone to over-fitting to training data or are ill-posed if there are more unknown parameters than observations. In both these cases, adding a regularization term  $P(\beta)$  can be beneficial. The estimated value of  $\hat{\beta}$  for the model becomes

$$\hat{\beta} = \operatorname{argmin}_{\beta} \sum_{i=1}^n \ell(y_i, f(\beta; X_i)) + \lambda P(\beta) \quad (3)$$

where  $\lambda$  is a free tuning parameter.

Well-known examples of regularization include  $L_1$  regularization  $P(\beta) = \|\beta\|_1$  (Lasso) [30], which promotes sparsity, or  $L_2$  regularization  $P(\beta) = \|\beta\|_2$  (Ridge regression) [20] which tends to keep parameters from growing excessively large. Both of these types of regularization can be viewed as making the topological statement that parameter weights should “cluster” around zero. A similar penalty from the topological point of view would simply encourage the set of all weights to form clusters, which can be accomplished by trying to minimize the sum of lengths of  $PD_0$  from a Rips or weak Alpha filtration on the weights.

Another class of well-known regularization schemes instead make an assumption about the topology of the set of parameters themselves, and penalize properties of the weights as a function on that space. Examples include penalties on a norm of a finite-difference derivative, such as total variation regularization  $P(\beta) = \|\nabla\beta\|_1$  [25], or penalties on the ordering of weights as seen in isotonic regression and its variants [31]. From the topological point of view, these regularization schemes encourage  $\beta$  to have a smaller number of local maxima and minima. A similar topological penalty

would simply penalize the number of maxima and minima directly which can be accomplished by minimizing the sum of lengths of  $\text{PD}_0$  from a level set filtration.

Penalty	Definition
L1	$\ \beta\ _1$
L2	$\ \beta\ _2$
TV	$\ \nabla\beta\ _1$
TV2	$\ \nabla\beta\ _2$
Top1	$\mathcal{E}(1, 0, 2; \text{PD}_0)$
Top2	$\mathcal{E}(1, 0, 4; \text{PD}_0)$

Figure 4: Abbreviation for penalties used for regularization of least squares problems.

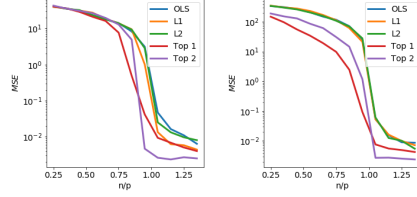


Figure 5: MSE of  $\hat{\beta}$  obtained using several regularization schemes as size of training set increases. Left: entries of  $\beta_*$  are drawn i.i.d. from  $\{-1, 0, 1\}$ . Right: entries of  $\beta_*$  are drawn i.i.d. from  $\{1, 2, 3\}$

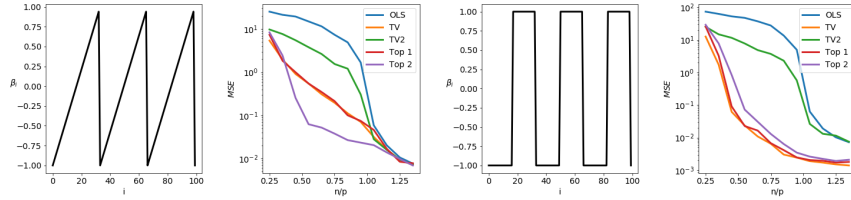


Figure 6: Left to right: Sawtooth  $\beta_*$ . MSE of linear prediction using  $\hat{\beta}$  obtained from several regularization schemes as size of training set increases. Boxcar  $\beta_*$ . MSE of linear prediction using  $\hat{\beta}$  obtained from same regularization schemes as size of training set increases.

In Figures 5 and 6, we compare different regularization schemes for several different linear regression problems. Data is generated as  $y_i = X_i\beta_* + \epsilon_i$ , where  $X_i \sim N(0, I)$ , and  $\epsilon_i \sim N(0, 0.05)$ .  $\beta_*$  is a feature vector with  $p = 100$  features, and an estimate  $\hat{\beta}$  is made from  $n$  samples by solving Equation 3 with the mean-squared error loss  $\ell(y_i, f(\beta; X_i)) = (y_i - X_i\beta)^2$  using different penalties, and  $\lambda$  is chosen from a logarithmically spaced grid on  $[10^{-4}, 10^1]$  via cross-validation for each penalty. We track the mean-squared prediction error for the estimate  $\hat{\beta}$  as the number of samples is increased. We also compare to the ordinary least-squares solution, with no regularization term, although if the solution is under-determined ( $n < p$ ), we take the smallest 2-norm solution.

In Figure 5, the features in  $\beta_*$  are chosen uniformly at random from three different values. On the left, those values are  $\{-1, 0, 1\}$ , and on the right,  $\{1, 2, 3\}$ . We consider  $L_1$  and  $L_2$  penalties, as well as two topological penalties using a weak-alpha filtration. The first is  $\mathcal{E}(1, 0, 2; \text{PD}_0)$ , and the second is  $\mathcal{E}(1, 0, 4; \text{PD}_0)$  which explicitly encodes that we expect three clusters. Both topological penalties are non-negative, and the first penalty is non-zero if  $\beta$  takes more than a single value, and the second penalty is non-zero if  $\beta$  takes more than three distinct values. In the case where  $\beta_*$  takes values in  $\{-1, 0, 1\}$ , the  $L_1$  and  $L_2$  penalties slightly outperform ordinary least squares, because while  $\beta_*$  is not truly sparse, some shrinkage seems beneficial. In the case where  $\beta_*$  takes values in  $\{1, 2, 3\}$ ,  $L_1$  and  $L_2$  clearly bias the estimate in an ineffective way and fail to outperform ordinary least squares. In contrast, the two topological penalties clearly do better in both cases.

In Figure 6, the features in  $\beta_*$  are chosen to have three local maxima when the features are given the line topology. On the left,  $\beta_*$  consists of three piecewise-linear sawteeth, and on the right,  $\beta_*$  consists of three piecewise-constant boxcars. The total variation penalty  $P(\beta) = \sum_{i=1}^p |\beta_{i+1} - \beta_i|$  and a smooth variant  $P(\beta) = (\sum_{i=1}^p |\beta_{i+1} - \beta_i|^2)^{1/2}$  are considered, as well as two topological penalties. The parameters of the topological penalties are identical to the previous example, but the penalties are now imposed on superlevel set diagrams of  $\beta$ . This means that instead of penalizing the number of clusters in the weights of  $\beta$ , we now penalize the number of local maxima. In the boxcar problem, total variation regularization does very well, as it encourages piece-wise linear functions, and the two topological penalties perform similarly. In the sawtooth problem, total variation does not do as well because  $\beta_*$  is no longer piece-wise constant, and interestingly the first topological penalty is similarly not as effective, while the second topological penalty performs similarly in both examples.

These examples demonstrate how topological information can be incorporated effectively to add regularization or incorporate prior knowledge into problems. Furthermore, they demonstrate how topological information can be directly encoded, such as penalties on the number of clusters or number of maxima of a function, in a natural way that is difficult to accomplish with more traditional schemes.

### 3.2 Incorporating Topological Priors in Generative Models

We now use the same topological priors to improve the quality of a deep generative neural network. We start with a Baseline-Generator, pre-trained in a GAN-setup on MNIST, and by training it for a few iterations with a topological loss, we arrive at an improved Topology-Generator. We provide comparisons with other methods applied to the Baseline-Generator.

A GAN as in [18] is trained on MNIST for 32,000 batch iterations with a batch size of 64 (this batch size is used throughout this section). The resulting generator (Baseline-Generator) produces reasonable output but with topological noise, see Figure 7 (a). The prior used to improve the Baseline-Generator is identical with that of Figure 3: that MNIST images should have one connected component in a superlevel set filtration. The loss function (topology loss) is  $\mathcal{E}(1, 0, 2; PD_0)$ .

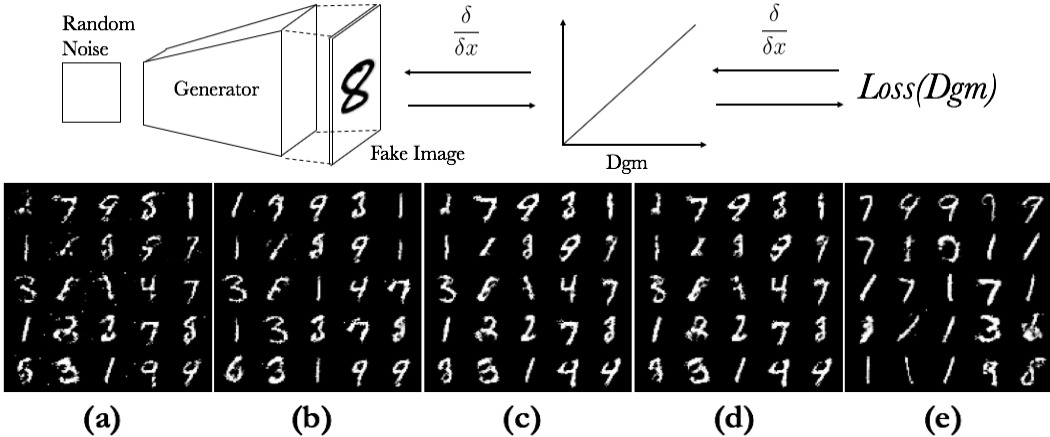


Figure 7: Top: Setup for computing topology loss and backpropagation. (a) Baseline-Generator. (b) Minimize the topology loss with respect to the latent space of Baseline-Generator. (c) Topology-Generator. (d) Train Baseline-Generator with topology-discriminator for 100 batch iterations. (e) Train Baseline-Generator in original GAN-setup for another 60,000 batch iterations

The setup in the top of Figure 7 is used to backpropagate to the latent space of Baseline-Generator, with generator weights fixed, in order to minimize the topology loss using SGD; the results can be seen in Figure 7 (b). Then, using the same setup, the Baseline-Generator’s weights are instead updated to minimize the topology loss; we train for 50 batch iterations to arrive at a new generator (Topology-Generator). The output of the Topology-Generator can be seen in Figure 7 (c).

For further qualitative comparisons, we train the Baseline-Generator for 100 batch iterations with a discriminator between features of the 0-dimensional persistence on MNIST images and the generator’s output. The features were sums of lengths of the  $k$  longest  $PD_0$  features for several choices of  $k$ , expressed as  $\mathcal{E}(1, 0, 2; PD_0) - \mathcal{E}(1, 0, 3; PD_0)$ ,  $\mathcal{E}(1, 0, 2; PD_0) - \mathcal{E}(1, 0, 4; PD_0)$ ,  $\mathcal{E}(1, 0, 2; PD_0) - \mathcal{E}(1, 0, 5; PD_0)$ , and  $\mathcal{E}(1, 0, 2; PD_0) - \mathcal{E}(1, 0, 11; PD_0)$ , with the results shown in Figure 7 (d). The output of a generator arrived at by training the Baseline-Generator in the original GAN-setup for another 60,000 batch iterations is shown in Figure 7 (e).

Evidently, the topology loss allows the generator to learn in only 50 batch iterations to produce images with a single connected component and the difference is visually significant. These results are similar to using a  $PD_0$ -aware discriminator, suggesting that our priors were valid. Updating only the latent space produces cleaner images but they still contain some topological noise. For a closer study, consider the linear interpolation in the latent space of the Baseline-Generator and Topology-Generator in Figure 8. The two different cases behave very differently with respect to the

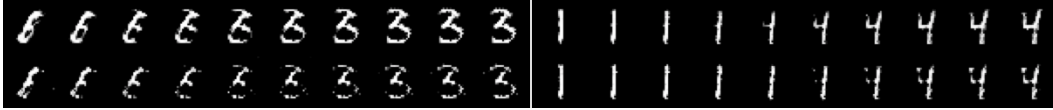


Figure 8: Linear interpolation in latent space. Top row: Topology-Generator. Bottom row: Baseline-Generator.

topology. The Baseline-Generator interpolates by letting a disconnected components appear and grow. The Topology-Generator tries to interpolate by deforming the number without creating disconnected components. This might be most obvious in the interpolation from “1” to “4” (Figure 8, right hand side) where the appended structure of the “4” appears as a disconnected component in the baseline but grows out continuously from the “1” in the topology-aware case.

We also quantitatively compare the Baseline-Generator and Topology-Generator to further investigate if any improvements have been made. We use the Minimal Matching Distance (MMD) and Coverage metric as advocated by [1] as well as the *Inception score* [26] (a convolutional neural network with 99% test accuracy on MNIST was used instead of the Inception model). The results can be seen in Table 9. MMD-Wass and COV-Wass use the same procedure as MMD-L2 and COV-L2 but instead of the L2 distance between images, the 1-Wasserstein distance between the 0-dimensional persistence diagrams of the images was used (see Section 2). The Topology-Generator shows improvements on all but one of these metrics. The table presents the averages of five computations of each metric, with test set sizes of 1,000 for L2 and Inception, and test sets sizes of 100 for Wasserstein.

Generator Evaluation					
Model	MMD-L2	COV-L2	MMD-Wass	COV-Wass	Inception
Baseline-Generator	28.0	0.05	3.1	0.03	4.6
Topology-Generator	<b>27.5</b>	<b>0.06</b>	<b>2.7</b>	<b>0.03</b>	<b>5.1</b>

Figure 9: Showing metrics for generator evaluation.

We extend this superlevel set filtration to 3D data in the form of voxel grids. As before, a baseline generator is obtained by training a GAN to generate voxel shapes as in [32] and its output after 1,000 epochs (or 333,000 batch iterations) can be seen in Figure 10 as the left hand members in each of the two pairs. The result of training with the topology loss (same as for images) for 20 batch iterations can be seen in Figure 10 as the right hand members in each of the two pairs. We claim no improvements on general metrics in this case but note that the generator is able learn to generate output with far fewer connected components.

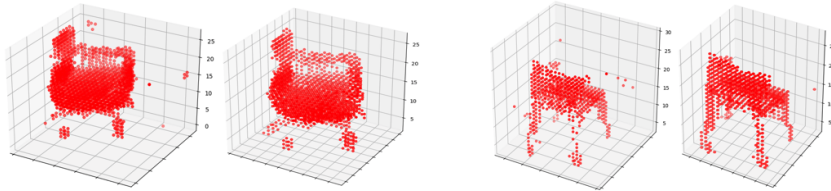


Figure 10: Left hand members of the pairs: before training with topology loss. Right hand members of pairs: after training with topology loss for 20 batch iterations.

### 3.3 Topological Adversarial Attacks

Our topological layer may also be placed at the beginning of a deep network. In contrast to other approaches that use persistence features for deep learning, we can use the fact that our input layer is differentiable to perform adversarial attacks, by backpropagating from the predictions back to the input image.

Since standard super-level set persistence is insufficient to classify MNIST digits, we include the orientation and direction information by computing the persistence homology during 8 directional sweeps. This is achieved by using the product of the image with fixed functions such as  $x$ ,  $y$ ,

$(x + y)/2 \dots$  etc, where  $x$  and  $y$  are the image coordinates, as the filtration value, one for each of the 8 directions,  $\mathcal{E}(p, q, 1; PD_k)$  for  $p$  and  $q$  ranging between 0 and 4 will result in 400 features for training the classification model

The model trained to classify the digits based on these topological features achieved 80-85 % accuracy. Next we performed gradient attack [17] to change the classification of the digit to another target class. We observe that it is harder to train adversarial images compared to CNNs and MLPs. The results are shown in Figure 12. A red outline indicates that the attack was successful. When the attack was conducted on 1,000 images, to retarget to a random class, it had 100% success rate on MLP and CNN models and 25.2% success rate on the TopModel.

When the adversarial attacks succeed the results sometimes offer insight as to how the model classifies each digit. For example in Figure 11, the left image is the original image of the digit 4, the right was trained to be classified as an 8; notice that two small holes at the top and bottom were sufficient to misclassify the digit. Several instances of the topological attacks provide similar interpretation. Attacks on MLP and CNN are qualitatively different, but further work is needed to gauge the extent and utility of such distinctions.

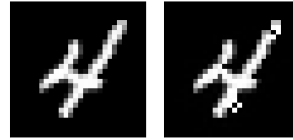


Figure 11: Example of Topological adversarial attack. Left is the original image, right image was optimized to be classified to be an 8, which introduced two 1 pixel holes.

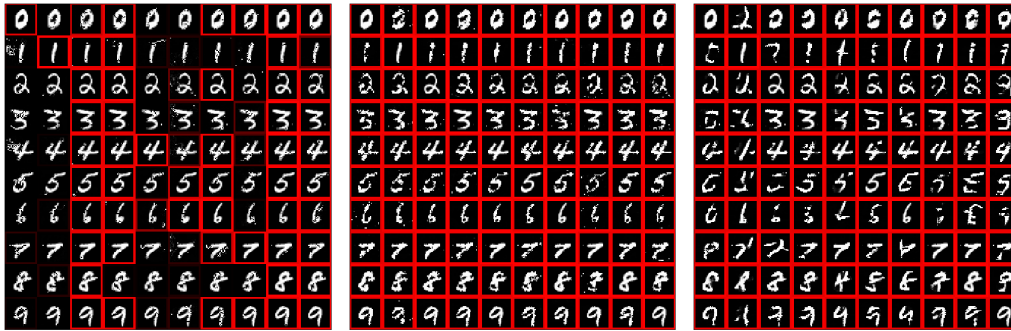


Figure 12: Topological adversarial attack on TopModel, MLPModel and CNNModel. Each  $(i, j)$ -cell with  $i, j \in \{0, 1, \dots, 9\}$  represents an attack on an image with label  $i$  to be classified with label  $j$ . Red outline indicates successful attack.

## 4 Discussion

We have presented a differentiable topology layer for machine learning as well as three novel applications that it makes possible. We enforced topological structure in Euclidean data, in images, and in the weights of machine learning models. We constructed a differentiable topology loss that allowed us to improve deep generative models. Finally, we compared gradient based adversarial attacks on deep models trained with topological features with the same attacks on CNNs and MLPs.

Our work only scratches the surface of the possible directions leveraging the differentiable properties of persistence. Without doubt such work will tackle problems beyond those we have presented here. Such work could include encouraging topological structure in intermediate activations of deep neural networks or using the layer in the middle of deep networks to extract persistence features where they may be more useful. However, many of the applications we have presented here also deserve further focus. For example, topological regularization, including the penalties we have presented, may have interesting theoretical properties, or closed form solutions. To the best of our knowledge, this is a first demonstration of persistence-based regularization of weights in a statistical model. Furthermore, training autoencoders with distances such as the bottleneck- or Wasserstein distance between persistence features might produce stronger results than the functions considered here. Finally, it might prove useful to use topological features to train deep networks that are more robust to adversarial attacks – however, as we show this will require additional work. Topology, in contrast to local geometry, is generally underexploited in machine learning, but changing this could benefit the discipline.



## 5 Acknowledgements

RBG and GC were supported by Altor Equity Partners AB and Harald and Jeanette Charitable Trust through Unbox AI (unboxai.org). BN was supported by the US Department of Energy, Contract DE-AC02-76SF00515. We are also grateful for Panos Achlioptas’ insights on the evaluation of our gen. Models.

## References

- [1] Panos Achlioptas, Olga Diamanti, Ioannis Mitliagkas, and Leonidas Guibas. Learning representations and generative models for 3D point clouds. In *Proceedings of the 35th International Conference on Machine Learning*, volume 80 of *Proceedings of Machine Learning Research*, pages 40–49, Stockholmsmässan, Stockholm Sweden, 10–15 Jul 2018.
- [2] Aaron Adcock, Erik Carlsson, and Gunnar Carlsson. The ring of algebraic functions on persistence bar codes. *Homology, Homotopy and Applications*, 18(1):381–402, 2016.
- [3] Rickard Brüel-Gabrielsson and Gunnar Carlsson. Exposition and interpretation of the topology of neural networks. *arXiv:1810.03234v2*, 2018.
- [4] Rickard Brüel-Gabrielsson, Vignesh Ganapathi-Subramanian, Primoz Skraba, and Leonidas Guibas. Topology-aware surface reconstruction for point clouds. *arXiv preprint arXiv:1811.12543*, 2019.
- [5] Gunnar Carlsson and Rickard Brüel-Gabrielsson. Topological approaches to deep learning. *arXiv:1811.01122*, 2018.
- [6] Gunnar Carlsson, Afra Zomorodian, Anne Collins, and Leonidas J Guibas. Persistence barcodes for shapes. *International Journal of Shape Modeling*, 11(02):149–187, 2005.
- [7] Anirban Chakraborty, Manaar Alam, Vishal Dey, Anupam Chattopadhyay, and Debdeep Mukhopadhyay. Adversarial attacks and defences: A survey. *arXiv preprint arXiv:1810.00069*, 2018.
- [8] Chao Chen, Xiuyan Ni, Qinxun Bai, and Yusu Wang. A topological regularizer for classifiers via persistent homology. In *Proceedings of Machine Learning Research*, volume 89 of *Proceedings of Machine Learning Research*, pages 2573–2582. PMLR, 16–18 Apr 2019.
- [9] Xi Chen, Yan Duan, Rein Houthoofd, John Schulman, Ilya Sutskever, and Pieter Abbeel. Infogan: Interpretable representation learning by information maximizing generative adversarial nets. In *Advances in neural information processing systems*, pages 2172–2180, 2016.
- [10] James R. Clough, Ilkay Oksuz, Nicholas Byrne, Julia A. Schnabel, and Andrew P. King. Explicit topological priors for deep-learning based image segmentation using persistent homology. *arXiv preprint arXiv:1901.10244*, 2019.
- [11] Tamal K Dey, Kuiyu Li, Chuanjiang Luo, Pawas Ranjan, Issam Safa, and Yusu Wang. Persistent heat signature for pose-oblivious matching of incomplete models. In *Computer Graphics Forum*, volume 29, pages 1545–1554. Wiley Online Library, 2010.
- [12] Herbert Edelsbrunner and John Harer. *Computational Topology - an Introduction*. American Mathematical Society, 2010.
- [13] Maxime Gabella, Nitya Afambo, Stefania Ebli, and Gard Spreemann. Topology of learning in artificial neural networks. *arXiv:1902.08160*, 2019.
- [14] Thomas Gebhart and Paul Schrater. Adversary detection in neural networks via persistent homology. *arXiv preprint arXiv:1711.10056*, 2017.
- [15] Thomas Gebhart and Paul Schrater. Adversarial examples target topological holes in deep networks. *arXiv preprint arXiv:1901.09496*, 2019.
- [16] Noah Giansiracusa, Robert Giansiracusa, and Chul Moon. Persistent homology machine learning for fingerprint classification. *arXiv preprint arXiv:1711.09158*, 2017.
- [17] Ian Goodfellow, Jonathon Shlens, and Christian Szegedy. Explaining and harnessing adversarial examples. In *International Conference on Learning Representations*, 2015.

- [18] Ian J. Goodfellow, Jean Pouget-Abadie, Mehdi Mirza, Bing Xu, David Warde-Farley, Sherjil Ozair, Aaron Courville, and Yoshua Bengio. Generative adversarial nets. In *Advances in neural information processing systems*, pages 2672–2680, 2014.
- [19] William H. Guss and Ruslan Salakhutdinov. On characterizing the capacity of neural networks using algebraic topology. *arXiv preprint arXiv:1802.04443*, 2018.
- [20] Arthur E. Hoerl and Robert W. Kennard. Ridge regression: Biased estimation for nonorthogonal problems. *Technometrics*, 12(1):55–67, 1970.
- [21] Christoph Hofer and et al. Deep learning with topological signatures. *31st Conference on Neural Information Processing Systems*, 2017.
- [22] Jen-Yu Liu, Shyh-Kang Jeng, and Yi-Hsuan Yang. Applying topological persistence in convolutional neural network for music audio signals. *arXiv:1608.07373*, 2016.
- [23] Adrien Poulencard, Primoz Skraba, and Maks Ovsjanikov. Topological function optimization for continuous shape matching. In *Computer Graphics Forum*, volume 37, pages 13–25. Wiley Online Library, 2018.
- [24] Bastian Rieck, Matteo Togninalli, Christian Bock, Michael Moor, Max Horn, Thomas Gumbsch, and Karsten Borgwardt. Neural persistence: A complexity measure for deep neural networks using algebraic topology. *arXiv preprint arXiv:1812.09764*, 2018.
- [25] Leonid I. Rudin, Stanley Osher, and Emad Fatemi. Nonlinear total variation based noise removal algorithms. *Physica D: Nonlinear Phenomena*, 60(1):259–268, 1992.
- [26] Tim Salimans, Ian Goodfellow, Wojciech Zaremba, Vicki Cheung, Alec Radford, and Xi Chen. Improved techniques for training gans. In *Proceedings of the 30th International Conference on Neural Information Processing Systems*, NIPS’16, pages 2234–2242, 2016.
- [27] Chi Seng Pun, Kelin Xia, and Si Xian Lee. Persistent-homology-based machine learning and its applications – a survey. *arXiv preprint arXiv:1811.00252*, 2018.
- [28] Primoz Skraba, Maks Ovsjanikov, Frederic Chazal, and Leonidas Guibas. Persistence-based segmentation of deformable shapes. In *Computer Vision and Pattern Recognition Workshops (CVPRW), 2010 IEEE Computer Society Conference on*, pages 45–52. IEEE, 2010.
- [29] Primoz Skraba, Gugan Thoppe, and D Yogeshwaran. Randomly weighted  $d$ - complexes: Minimal spanning acycles and persistence diagrams. *arXiv preprint arXiv:1701.00239*, 2017.
- [30] Robert Tibshirani. Regression shrinkage and selection via the lasso. *Journal of the Royal Statistical Society, Series B*, 58(1):267–288, 1996.
- [31] Ryan J. Tibshirani, Holger Hoefling, and Robert Tibshirani. Nearly-isotonic regression. *Technometrics*, 53(1):54–61, 2001.
- [32] Jiajun Wu, Chengkai Zhang, Tianfan Xue, Bill Freeman, and Josh Tenenbaum. Learning a probabilistic latent space of object shapes via 3d generative-adversarial modeling. In *Advances in neural information processing systems*, pages 82–90, 2016.

## 6 Appendix

### 6.1 Topological definitions

In this section, we give the precise definitions of the required notions – this should not be considered as an exhaustive introduction, but rather our goal is to give precise definitions to the concepts used in the paper.

**Definition 6.1.** A  $k$ -dimensional simplex is the convex combination of  $k + 1$  vertices.

We only consider the situation where the vertices correspond to point in a sufficiently nice ambient space, usually  $\mathbb{R}^d$  so that a geometric realization of simplices exists as a subset of the ambient space. Simplices are used to represent a space, but must satisfy some additional constraints so that they form a *simplicial complex*.

**Definition 6.2.** A simplicial complex  $\mathcal{X}$  is a collection of simplices such that

1. For every simplex  $\sigma$  in  $\mathcal{X}$ , every face  $\tau \subseteq \sigma$  is also in  $\mathcal{X}$ .
2. For any two simplices  $\sigma_1$  and  $\sigma_2$ ,  $\tau = \sigma_1 \cap \sigma_2$  is a face of both  $\sigma_1$  and  $\sigma_2$ .

These can be thought of as higher dimensional analogs of graphs – conversely, a graph is a 1-dimensional simplicial complex.

To define homology, we first construct a *chain group*. In our setting, the  $k$ -th chain group  $C_k(\mathcal{X})$  is the freely generated group generated by  $k$ -dimensional simplices. Importantly, there exists a boundary homomorphism

$$\partial_k : C_k(\mathcal{X}) \rightarrow C_{k-1}(\mathcal{X})$$

such that  $\partial \circ \partial = 0$ . Homology can then be defined as

$$H_k(\mathcal{X}) = \frac{\ker \partial_k}{\text{im } \partial_{k+1}}$$

We consider homology computed over fields, in which case the homology groups are vector spaces. Rather than only consider one simplicial complex  $\mathcal{X}$ , we can consider an increasing sequence of simplicial complexes, called a *filtration*  $\mathcal{X}_0 \subseteq \mathcal{X}_1 \subseteq \dots \subseteq \mathcal{X}_N$ . The requirement is that each  $\mathcal{X}_i$  is itself a simplicial complex. We consider the filtration function  $f : \mathcal{X} \rightarrow \mathbb{R}$  such that each sub/super-level set  $f^{-1}(-\infty, \alpha]$ , resp.  $f^{-1}[\alpha, \infty)$  form a filtration in parameterized by  $\alpha$ . Under appropriate finiteness conditions, which are always satisfied for finite simplicial complexes [12].

**Theorem 6.3.** If homology is computed over a field, then the homology of a filtration admits an interval decomposition. The interval decomposition is direct sum of rank 1 elements which exists over an interval  $[b, d)$ .

In our setting, whether the intervals are open or closed is not important so we suppress this aspect of the notation. This collection of intervals is the *persistence diagram*.

**Definition 6.4.** A persistence diagram is a collection of points  $(b_i, d_i)$ , possibly with repetition, along with the diagonal  $\Delta$ , i.e. all points such that  $b = d$ .

The diagonal plays an important part in the definition of distances between diagrams. The main distance we consider is the  $p$ -Wasserstein distance between two diagrams

$$W_p(\text{PD}_k(f), \text{PD}_k(g)) = \inf_{\varphi} \left( \sum_{p \in \text{PD}_k(f)} \|p - \varphi(p)\|^p \right)^{1/p}$$

where  $\varphi$  is a bijection. This can be viewed as an optimal transport problem, points must either be matched to the other diagram or the diagonal. This can be formulated as a classical linear program if we add to each diagram the projection of the other diagram to the diagonal

$$\text{proj}(d, b) = \left( \frac{d+b}{2}, \frac{d+b}{2} \right)$$

In other words, we can consider the optimal transport problem between  $\text{PD}(f) \cup \text{proj}(\text{PD}(g))$  and  $\text{PD}(g) \cup \text{proj}(\text{PD}(f))$  where the distance between any two points on the diagonal is 0.

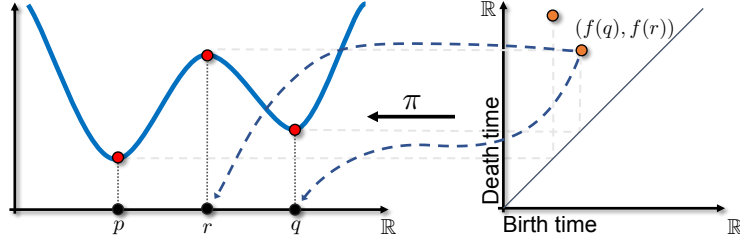


Figure 13: A one dimensional example of a persistence diagram and the inverse map  $\pi$ . The function on the left has critical points at points  $p$ ,  $r$  and  $q$ . The local minima create components in the sub-level sets and so represent birth times ( $x$ -axis), while the maxima kills one of the components (the younger one) and so is a death time ( $y$ -axis). The inverse map for a point in the diagram returns the corresponding critical points/simplicies.

One of the core techniques in this paper is to compute the gradient of an energy function with respect to some parameters. This is possible through the definition of an inverse map

$$\pi_f(k) : \{b_i, d_i\}_{i \in \mathcal{I}_k} \rightarrow (\sigma, \tau)$$

This map is unique and well defined in the case of when a filtration is a total order, i.e. the simplices are totally ordered in the filtration. This is never the case in our scenarios, where the simplices only form a partial order. However this can be resolved by extending the partial to a total order either deterministically or randomly, see [29] for a formal proof and description of how this can be done.

As is the case in our setting, the filtration is not defined directly on the simplices but rather derived from either functions on the vertices or depend on some property of the vertices, e.g. the coordinates of the points that the vertices correspond to. In this case, we require an additional inverse map from simplices to a collection of vertices. This is described in the main paper for two scenarios which we use in the applications. Once both inverse maps are defined, the gradient can be defined in the standard way using the chain rule.

## 6.2 Comparison

In this paper we use both super-level set filtrations as well as Vietoris-Rips and weak-Alpha filtrations. Figure 14 provides an illustrative comparison of super-level set filtration (on the left) and a Rips filtration (on the right). The digit "9" viewed in terms of the super-level set of its pixel values has one clear connected component and one clear ring, which can be read from the corresponding persistence diagrams. However, the super-level set filtration does not take into consideration distance along the grid and a small (in the 2D sense) hole can be very large from the superlevel set perspective. In the Rips case we lay out all the pixelvalues in a 3D space and use the euclidean distance. Here there are many more connected components at small to medium filtration values, and the same is true for the number of rings. The Rips does not merely pick up the obvious ring in the "9" but also rings that are formed with respect to the vertical axis.

## 6.3 Explore latent space

In this paper we backpropagate to the latent space of generative models (query the latent space) in order to improve on them. However, the ability to topologically query the latent space may not only be used to give us more topologically desirable output but also to explore the nature of the latent space. Consider Figure 15 that consists of images produced by a trained InfoGAN-generator [9]. The type of digit closest to a "2" with a loop on the bottom is arguably a digit "2" without such a loop. However, when we backpropagate to remove the ring we get something that does not look like any MNIST digit. Similarly, if we remove the ring in the digit "6" we get something that does not look very much like any MNIST digit. This gives some indications that the latent space learned by the InfoGAN is relatively topologically flexible.

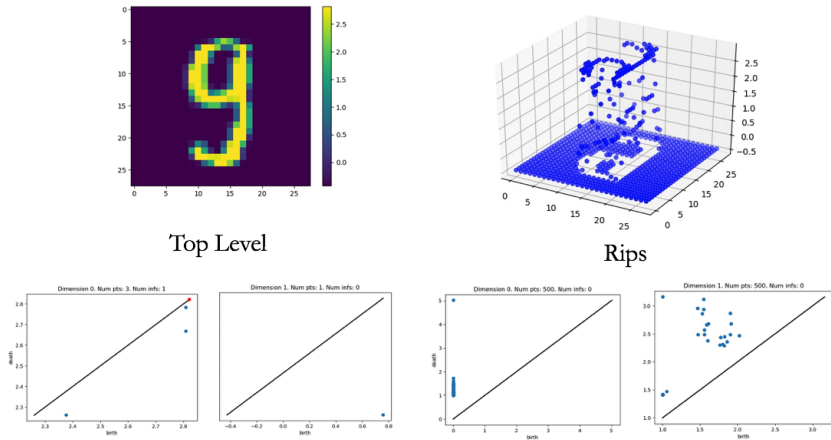


Figure 14: Compare top level set with Rips filtration

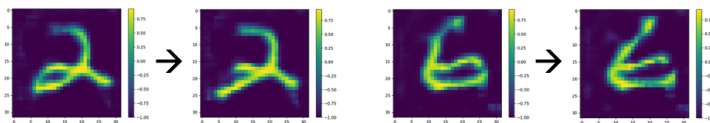


Figure 15: Infogan query

## 6.4 Topological Mapping

In this paper we train and experiment with networks that use persistence as input. However, with a differentiable layer we can put the persistence computations anywhere in the network. Sometimes it is useful to put certain layers in the middle of a deep network. For example in domain transfer we often want to create a mapping where features will be more useful. The setup might look like in the Figure 16. We do a simpler setup where we train a network to use superlevel persistence features to

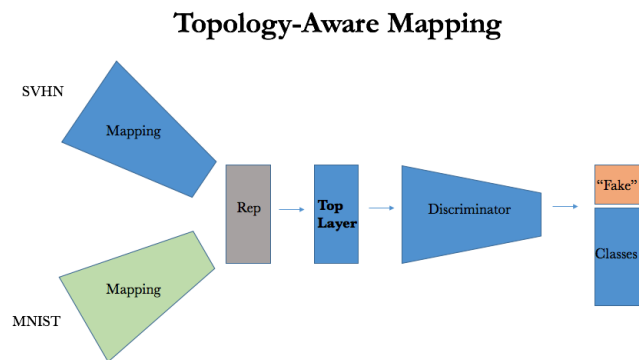


Figure 16: Topological mapping

classify the naive  $PD_1$ -features of MNIST which we define for "1", "2", "3", "4", "5", "7" as zero, for "0", "6", "9" as one, and for "8" as two. We are able to get a 84% accuracy. However, by putting two convolutional layers (the mapping) which maintain the dimensionality of the input before our Topology Layer, we get the results shown in Figure 17 where we ultimate improve our accuracy to 86%. In this case, it seems as if the mapping thickens the digits in the images in order to remove topological noise.

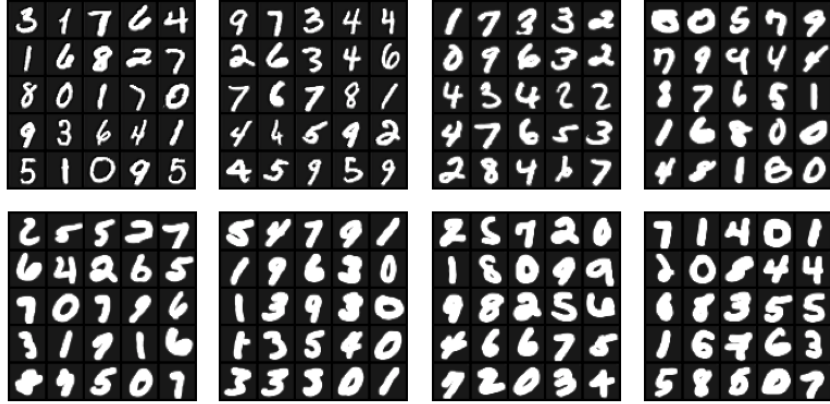


Figure 17: Intermediate Representation in topological mapping

## 6.5 Topological Adversarial Attacks

### 6.5.1 Features for classification model

In order to train a classification model using only topological features we must include orientation and directional information into the persistence homology features. This can be achieved by using custom filtration constructed in the following way. First we define 8 directional functions

$$g_\theta(x, y) = \cos(\theta)x + \sin(\theta)y \quad \theta = 0, \pi/4, \pi/2, \dots, 7\pi/4$$

These functions are shifted and scaled so that in the domain of the image, they range from 0 to 1. If  $I(x, y)$  is the input image, then the filtrations are given by

$$f_{\theta_i}(x, y) = I(x, y)g_{\theta_i}(x, y)$$

Persistence diagrams of dimensions 0 and 1 are computed for each filtration. We then compute 25 features on each persistence diagram given by  $\mathcal{E}(p, q, 0; \text{PD})$ , for  $p$  and  $q$  ranging between 0 and 4, thus totalling 400 features.

## 6.6 Regularization Sparsity Visualization

In Figure 18 we see the Rips  $\text{PD}_0$  diagram for the weights of a logistic regression model without (left) and with (right) L1 regularization. As the test accuracy improves, we see that the persistence diagram changes as well.

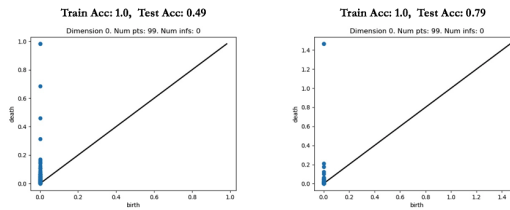


Figure 18: Rips and generalization